Available online at www.sciencedirect.com
SCIENCE DIRECT®
Coordination Chemistry Reviews 238–239 (2003) 167–185
COORDINATION CHEMISTRY REVIEWS
www.elsevier.com/locate/ccr

Thermal and optical electron transfer involving transition metal complexes: insights from theory and computation

Marshall D. Newton *

Chemistry Department, Brookhaven National Laboratory, Upton, NY 11973-5000, USA

Received 13 March 2002; accepted 5 September 2002

Contents

* Tel.: +1-631-344-4366; fax: +1-631-344-5815
E-mail address: newton@bnl.gov (M.D. Newton).

PII: S0010-8545(02)00253-9

Abstract

Current theories of electron transfer (ET) kinetics in conjunction with techniques of computational quantum chemistry are reviewed and applied to the analysis of thermal and optical ET processes involving transition metal complexes (TMCs). The roles of geometrical and electronic structure in controlling the relevant energetics and electronic coupling are discussed, and a number of limiting cases of kinetic behavior are displayed. Particular attention is paid to the formulation of the initial and final states involved in the ET, including the consequences of near-degeneracy and spin–orbit coupling. The roles of metal/ligand mixing and other types of 'mediation' of donor/acceptor coupling by molecular spacers are noted and illustrated with calculated results. An example of a detailed computation of activation parameters is also presented, including entropic effects and nuclear tunnelling.

Keywords: Electron transfer; Energy surfaces; Electronic Coupling Elements; Activation parameters

1. Introduction

Coordination complexes continue to play a central role in the ongoing field of electron transfer (ET) chemistry, one characterized by rapidly expanding mechanistic understanding [1], whose implications for design of novel systems and processes of technological significance (e.g. molecular electronics and sensor devices) are being intensively pursued [2,3]. Numerous recent reviews dealing with electronic and energetic factors of relevance to thermal and optical ET processes have appeared, offering an overview of experimental, theoretical, and computational means of probing basic ET mechanisms [4–9]. It is well recognized that these probes working in tandem provide very powerful tools for quantitative elucidation of the different factors controlling ET dynamics and for the formulation of compact predictive models. In the present review we focus on a selected set of mechanistic issues of particular importance for ET systems based on transition metal complexes (TMC) (Scheme 1). Because of the complexity of the electronic structure of TMCs, reliable quantum chemical modeling remains a major challenge, but a number of promising computational approaches are now available for treating ET systems [10–28], and rapid expansion of such capability is proceeding steadily, based on ab initio and density functional techniques [29–32].

Basic models for energetics and kinetics are presented in Section 2. The formulation of initial and final electronic states and associated electronic coupling elements is given in Section 3, followed by a number of illustrative computational applications in Section 4.

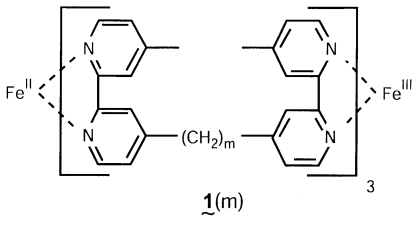

Scheme 1.

These applications offer detailed examples of calculated electronic coupling elements and activation parameters, showing the consequences of ligand–metal mixing, structural variation, and alternative choices of initial and final states on the overall efficiency of the ET process, and the extent to which meaningful contact may be established between theory and experiment. Unifying features of thermal and optical ET are emphasized.

2. Kinetic framework

The basic ingredients of kinetic theory for thermal ET, and the closely related theory for optical ET, have been covered in detail in a number of reviews [4,5,33–40]. Here we simply provide enough background to permit an adequate appreciation of the various applications of theory to ET involving TMCs in later sections. The first task in modeling ET is to characterize the initial (ψ_i) and final (ψ_f) electronic states in the process (plus any other, intermediate states which may be significant). For present purposes we assume that these states are known, and furthermore, we confine the treatment to a simple two-state approximation, TSA (i.e. based solely on ψ_i and ψ_f). In subsequent sections, theoretical formulations of ψ_i and ψ_f are discussed (Section 3), and procedures for dealing with multiple electronic states (i.e. beyond the TSA, as for example in cases of near-degeneracy) are addressed.

The ET processes dealt with here are important examples of a larger class of electronic processes involving local donor (D) and acceptor (A) sites, and including nominally 'two-particle' (e.g. Dexter energy transfer and magnetic exchange) as well as 'one-particle' process such as electron (ET) and hole transfer (HT). Unless noted otherwise we use the term 'electron transfer' generally to refer to both ET and HT. A schematic representation of corresponding thermal and optical ET processes at the level of the TSA is given in Fig. 1, showing free energy profiles of the initial and final states along the reaction coordinate (η). The choice of reaction coordinate is discussed below. The initial and

final states are denoted generically as DBA and D^+BA^- to reflect the fact that in typical situations it is convenient to represent the D/A interaction as being mediated by an intervening molecular bridge (B) or 'spacer.' For intramolecular ET, e.g. as in binuclear TMCs, the entire DBA assembly is a bonded molecular system. The decomposition into D, B and A units is somewhat arbitrary, guided by convenience or chemical intuition (e.g. metal ions, with or without their immediate coordination shells, may serve as local D and A sites, with the remainder of the assembly serving as the bridge or tether). In cases of bimolecular ET between TMCs it may be useful to view the metal (M) ions as the local D and A sites, with the ligands (L) in direct contact serving collectively as the bridge (B) [13]. Examples of both situations are considered below.

The thermal process involves activation, i.e. a thermal fluctuation which brings the system from the equilibrium initial (reactant) state to the transition state (TS), the configuration in which the donor and acceptor are 'resonant.' Subsequent thermal deactivation takes the system to the final (product) state. In the optical ET process, the photon energy allows energy conservation in the vertical process, typically occurring from the equilibrium configuration of the state of lowest energy (D^+BA^- in Fig. 1).

Thermal and optical ET processes may be formulated in terms of a common theoretical model [41]. In this section we present explicit rate constant expressions for the thermal process (k_{ET}). We note that thermal processes may occur either in ground or excited state manifolds, provided the initial state ψ_i (either ground or photoexcited) is thermally equilibrated with respect to the nuclear modes of the system [38]. Electronic relaxation between excited electronic manifolds may also occur [9b]. For example, in the case of photoexcited TMCs, ψ_i may be a triplet state originating (via intersystem crossing) from an initially excited singlet.

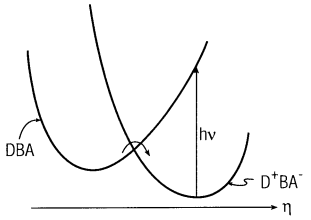

Fig. 1. Schematic representation of optical and thermal et, corresponding, respectively, to the vertical transition with excitation energy $h\nu$ and passage through the transition-state (or crossing) region. In experimental studies, the thermodynamically stable state, which is the final state in the thermal ET process, generally serves as the initial state in the corresponding optical process. The optical and thermal processes are generally understood to involve transitions, respectively, between pairs of adiabatic and diabatic states (see Section 2). In the weak-coupling situation depicted in the figure, the distinction between adiabatic and diabatic energy profiles (due to quantum mechanical mixing) is suppressed.

For thermal ET, ψ_i and ψ_f are nonstationary states, denoted below as 'diabatic' and corresponding to initial and final charge-localized states [4].

The nuclear modes for each electronic state may be represented classically or quantum mechanically, a decision generally made (for a given mode) on the basis of the magnitude of $h\nu$ (where ν is the relevant vibrational frequency) in relation to k_BT [38]. Solvent modes are generally treated as a low-frequency classical continuum, whereas higher frequency molecular modes of the 'solute' (DBA) may be treated quantum mechanically, and in either case, the modes are generally assumed to be harmonic [38,42]. The labels 'inner sphere' and 'outer sphere' are often used to distinguish the solute and solvent parts of the overall ET system, especially in cases of ET between mononuclear coordination complexes. This review is confined to so-called 'outer-sphere ET' [33–35], in which the formal bonding within the inner spheres is maintained throughout the reaction, even though substantial shifts in inner shell equilibrium coordinates may occur, thus contributing along with solvent to the total reorganization energy.

2.1. Energetics in the weak coupling limit

We now adopt as the definition of the ET reaction coordinate, η, the vertical free energy difference for ψ_i and ψ_f at an arbitrary configuration of the nuclear coordinates [4,38]. This definition is the conventional one for ET in polar media, and is especially convenient in view of the collective nature of the medium contribution to the reaction coordinate [43]. The energy quantities needed to formulate k_{ET} in the standard framework of transition state theory (TST) are given in terms of the free energy profiles shown in Fig. 1 and displayed in greater detail in Fig. 2. These free energy profiles are defined such that at a given value of η, the free energy ($G_i(\eta)$ or $G_f(\eta)$) is minimized subject to this constraint. We emphasize that this definition of reaction coordinate is not unique, and any linear function of η, as defined above, is an acceptable alternative [4]. Fig. 2 is drawn for the limiting case of diabatic states [4,36], where G_i and G_f intersect in a cusp (the consequences of finite coupling between these states are pursued below). The two profiles are often approximated as shifted parabolas of equal curvature (the case of 'linear response'), although Fig. 2 is not limited by this restriction. The horizontal and vertical shifts of the free energy minima of ψ_i and ψ_f lead, respectively, to the kinetically crucial reorganization free energies λ_i and λ_f and reaction driving force ($-\Delta G^\circ$). For weakly-coupled D and A sites (the non-adiabatic limit presented below), the ET process is Franck–Condon controlled and the actual charge transfer can occur only at the crossing point ($\eta^\dagger$) characterized by activation energy, $G^\dagger$, a consequence of the horizontal shift of equilibrium

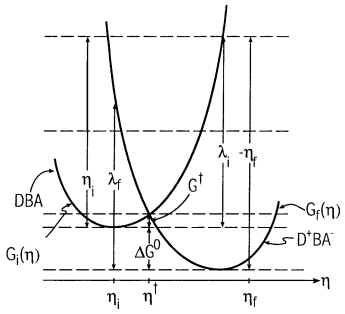

Fig. 2. Free energy profiles along the reaction coordinate (η) for the initial and final diabatic states, indicating the reorganization energy (λ), activation free energy ($G^\dagger$), and reaction driving force ($-\Delta G^\circ$). In a linear system, with parabolic profiles of equal curvature and $\lambda_i = \lambda_f = \lambda$ (as implied by the figure) the free energy change ΔG° can be equated to the gap between the minima of the two (constrained) free energy profiles [4] (a near equality is expected in general, e.g. as found in Ref. [14]), and the vertical energy gap (η_i) at the equilibrium configuration for the initial state (DBA) is equal to $\lambda+\Delta G^\circ$ [4]. Correspondingly, the final-state (D^+BA^-) gap ($-\eta_f$) is given by $\lambda-\Delta G^\circ$.

coordinates ($\eta_i \neq \eta_f$). While η may in principle have contributions from all the modes of the system (solute and solvent), in practice it may typically be represented to good approximation in terms of a small sub-set of modes: e.g. an antisymmetric combination of ML breathing modes and a solvent polarization mode [4,33,34].

For a harmonic system (shifted parabolas of fixed curvature), simple Marcus expressions [34] relate the various quantities displayed in Fig. 2:

$$\eta_i = \lambda + \Delta G^\circ \tag{1a}$$

$$\eta_f = \lambda - \Delta G^\circ \tag{1b}$$

$$G^\dagger = (\eta_i)^2/4\lambda = (\lambda + \Delta G^\circ)^2/4\lambda \tag{2}$$

where

$$\lambda \equiv \lambda_i = \lambda_f$$

and λ has the form $k_\eta(\eta_i - \eta_f)^2/2$. The total reorganization energy λ may be decomposed into a sum of individual terms of the same form,

$$\lambda = \sum_j \lambda_j \tag{3}$$

based on those normal coordinates (q_j) of the harmonic system which undergo a shift in equilibrium coordinate value in the course of the ET process. For the solvent polarization contribution, λ_s, an equivalent expression in terms of dielectric continuum theory was derived by Marcus [43a]. It has recently been determined (from both theory [44] and experiment [45,46] that λ_s for ET in polar solvents may have an appreciable positive entropy contribution, λ_S, given by

$$\lambda_S = -\mathrm{d}\lambda_s/\mathrm{d}T \tag{4}$$

The quadratic free energy relationship between $G^\dagger$ and ΔG° (Eq. (2)) may be approximated as a conventional linear free energy relationship when $|\Delta G^\circ|/\lambda \ll 1$, in contrast to more strongly exothermic processes in the 'normal region' ($-\Delta G^\circ < \lambda$) or the 'inverted region' ($-\Delta G^\circ > \lambda$) [34]. In the latter case, optical ET may occur in absorption or emission, and the Stokes shift is given by 2λ [4,34,41].

The activation energetics must now be supplemented by a consideration of the coupling between ψ_i and ψ_f, without which no ET will occur. While the overall coupling may be a complex vibronic phenomenon [38,42], a quantity of central importance is the electronic coupling matrix element,

$$H_{if} = \int \psi_i H_{el} \psi_f \mathrm{d}\tau \tag{5}$$

where H_{el} is the electronic Hamiltonian of the system. In general, H_{if} will vary with nuclear coordinates, in which case H_{if} may either be evaluated at the TS ($\eta^\dagger$), or more detailed account may be taken of coordinate fluctuations (see below). Coordinate dependence is neglected in the Condon approximation [47].

2.2. Transition state theory

The TST thermal rate constant for unimolecular ET may be represented as [33]

$$k_{ET} = \nu_n \kappa_{el} \kappa_n \tag{6}$$

where the effective fraction of the reactant species in the TS ($\eta^\dagger$) is given by the nuclear factor, κ_n, and the fraction of systems activated species which successfully pass through the crossing region and on to products per unit time is given by the product of an effective nuclear frequency, ν_n, and the electronic transmission factor, κ_{el}. The details of κ_{el} and κ_n depend on the quantum mechanical features of the electronic and nuclear manifolds. For bimolecular ET processes the overall second-order rate constant must be constructed in terms of the unimolecular k_{ET} evaluated for the relevant range of inter-reactant coordinates (translational and orientational) and the appropriate distribution function for such coordinates. When both reactants are charged, this function will involve the electrostatic work to bring the reactants to finite separation [34].

For classical nuclear motion and sufficiently strong electronic coupling (H_{if}), the adiabatic limit discussed below, we have [33],

$$\kappa_{el} = 1$$

$$\kappa_n = \exp(-G^\dagger/k_B T) \tag{7}$$

where k_B is the Boltzmann constant. If $G^\dagger$ includes an entropic term, $S^\dagger$, then the activation enthalpy is distinct from $G^\dagger$ [14],

$$G^{\dagger} = H^{\dagger} - TS^{\dagger}$$

$$S^{\dagger} = -\mathrm{d}G^{\dagger}/\mathrm{d}T \tag{8}$$

For the condensed phase ET processes of interest in the present study, the distinction between $H^{\dagger}$ and the activation energy (E_a) will be neglected. We may now cast k_{ET} (Eq. (6)) in Arrhenius form,

$$k_{ET} = A\ \exp(-H^{\dagger}/k_B T) \tag{9}$$

where

$$A = \nu_n \kappa_{el} \exp(S^{\dagger}/k_B) \tag{10}$$

$$H^{\dagger} = -k_B \mathrm{d}(\ln k_{ET})/\mathrm{d}(1/T) \tag{11}$$

The prefactor is either constant or varies weakly with temperature, depending on the details of the kinetic model (see below). When nuclear tunnelling is significant (arising from high frequency modes where $h\nu \gtrsim k_B T$), κ_n may include a tunnelling factor, Γ_n, reflecting a lowering of the effective activation free energy, $G^{\dagger}$, relative to the classical value, $G^{\dagger}_{cl}$ [4,14,33,38]

$$\kappa_n = \Gamma_n \exp - G^{\dagger}_{cl}/k_B T \tag{12}$$

where

$$\Gamma_n \equiv \exp(-(G^{\dagger} - G^{\dagger}_{cl})/k_B T)$$

(in general, the superscript 'cl' is suppressed below, except as needed to avoid ambiguity). Note that in general, Γ_n is temperature dependent, thus contributing to both $H^{\dagger}$ and A (see Eq. (9)).

The non-adiabatic kinetic regime (denoted by the superscript 'na'), pertains when electronic coupling is strongly 'rate limiting' (i.e. $\kappa_{el} = \kappa^{na}_{el} \ll 1$), and expressions for κ_{el} may be obtained on the basis of the golden rule [4,33]. For classical, harmonic nuclear motion in the general case, the Landau–Zener model yields [33],

$$\kappa_{el} = 2(1 - \exp(-\gamma/2)/(2 - \exp(-\gamma/2)))$$

where

$$\gamma = \{(2\pi H^2_{if}/\hbar)/(4\pi k_B T \lambda)^{1/2}\}/\nu_n \tag{13}$$

Thus, κ_{el} is seen to range from zero to unity as H_{if} increases in magnitude (for given values of T, λ and ν_n). In the nonadiatic limit, $\kappa_{el} = \kappa^{na}_{el} \ll 1$, we obtain from Eq. (13),

$$\kappa^{na}_{el} \cong \gamma \tag{14}$$

We thus have (see Eqs. (6) and (7)),

$$k^{na}_{ET} = \{(2\pi H^2_{if}/\hbar)/(4\pi k_B T \lambda)^{1/2}\}(\exp(-G^{\dagger}/k_B T)) \tag{15}$$

where the bracketed quantity corresponds to $\nu_n \kappa^{na}_{el}$. A regrouping of the factors yields the alternative form,

$$k^{na}_{ET} = (2\pi H^2_{if}/\hbar)\ \ (\mathrm{FCWD}) \tag{16}$$

where the 'Franck–Condon weighted density of states', FCWD, is given by

$$\mathrm{FCWD} = \exp(-G^{\dagger}/k_B T)/(4\pi\lambda k_B T)^{1/2} \tag{17}$$

The lineshape of the corresponding optical ET process is given by an analogous expression for FCWD, in which $G^{\dagger}(\Delta G^{\circ})$, for example as given in Eq. (2), is replaced by $G^{\dagger}(\Delta G^{\circ} \pm h\nu)$ for absorption (−) and emission (+), and ν is the variable optical frequency [41].

In view of the $T^{-1/2}$ factor in Eqs. (15) and (17), fitting of non-adiabatic rate constants in terms of the Arrhenius form (Eq. (9)) may be applied to the scaled quantity, $k_{ET}T^{1/2}$. When some of the nuclear modes are quantized, we find that in addition to the reduction of $G^{\dagger}$ due to tunnelling, as discussed above, the classical quantity, $k_B T\lambda$, in the prefactor of Eq. (15) is replaced by a somewhat smaller quantized counterpart [4,14,33].

For electronic coupling (H_{if}) of arbitrary strength, the magnitude of κ_{el} positions a given ET process relative to the non-adiabatic ($\kappa_{el} \ll 1$) and adiabatic ($\kappa_{el} \sim 1$) limits [38,42]. Since κ_{el} reflects the joint influence of ν_n, λ, T and H_{if}, a given ET process will, for example, move toward the nonadiabatic limit as ν_n increases, if all other quantities are kept fixed. An adiabatic process may be understood in terms of dynamics on single energy surface, whereas non-adiabatic dynamics intrinsically involves more than one energy surface [4]. These situations may be analyzed either in terms of the 'diabatic states' (ψ_i and ψ_f) employed in the discussion so far (with the associated cusp-like crossing point and coupling element, H_{if}), or in the alternative representation provided by the corresponding 'adiabatic states' (denoted ψ_1 and ψ_2), which by definition are eigenstates of H_{el}, manifesting an avoided crossing in the TS region [4,48] (see Fig. 3). Nonadiabatic ET occurs 'suddenly' (Franck–Condon control) in a narrow 'reaction zone' (Fig. 3a), during relatively rare events ($\kappa_{el} = \kappa^{na}_{el} \ll 1$) when the system hops between diabatic states or, equivalently, remains in the lower adiabatic state during a 'crossing'. Adiabatic ET occurs gradually in a broader reaction zone, with the system remaining in the lower adiabatic state (Fig. 3b). Adiabatic states at the crossing (i.e. at the point, $\eta^{\dagger}$, where the diabatic curves cross) are separated by a gap [4,33,35],

$$\Delta E_{12} = 2|H_{if}| \tag{18}$$

The avoided crossing associated with adiabatic states also affects the activation free energy, $G^{\dagger}$. For example, in the case of a thermoneutral process ($\Delta G^{\circ} = 0$), Eq. (2) may be refined as follows [33]:

$$G^{\dagger} = (\lambda - 2|H_{if}|)^2/(4\lambda) \tag{19}$$

A double-well adiabatic energy profile of the type displayed in Fig. 3, will occur provided that the coupling magnitude ($|H_{if}|$) is below a threshold determined by λ and ΔG°. For the special case ($\Delta G^{\circ} = 0$), the constraint is simply, $\Delta E_{12} < \lambda$. The more general situation is discussed in [35]. The double-well situation corresponds

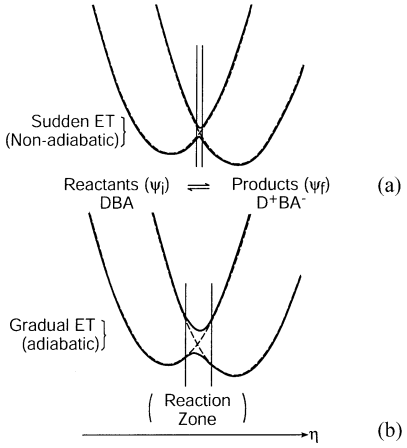

Fig. 3. Schematic depiction of the limits of (a) weak (nonadiabatic) and (b) strong (adiabatic) coupling. The dashed (solid) lines refer to diabatic (adiabatic) surfaces. The vertical bars denote the 'reaction zone' in which D and A sites are close to resonance [57].

to some degree of charge localization (i.e. for the adiabatic states, as well as for the diabatic states, which by construction are charge-localized [47]), and is generally denoted as belonging to the Robin–Day Class II [49] (especially for mixed-valence binuclear TMCs) in contrast to the delocalized, single-well Robin–Day Class III [49]. The cases considered in Section 4 are all of the Class II type.

2.3. Features of the coupling element (H_{if})

Some insight into the physical nature of H_{if} may be obtained by decomposing it into separate factors. We mention three examples.

2.3.1. Orbital versus many-electron wavefunction coupling

The quantity, H_{if}, while properly viewed in general as a matrix element involving many-electron states, ψ_i and ψ_f, is typically found to be closely approximated by an orbital matrix element, H_{DA},

$$H_{if} = S_{if} H_{DA} \sim H_{DA} \tag{20}$$

where D and A are the donor and acceptor orbitals in which the transferring electron is primarily localized, respectively, in ψ_i and ψ_f, and where the overlap integral S_{if} (an electronic 'Franck–Condon factor' reflecting the influence of the $(n-1)$-electron 'core' of the n-electron ET system) has been found in a number of theoretical studies to be close to unity ($S_{if} \gtrsim 0.9$) [4,13,36].

2.3.2. Spin-dependence

When ET occurs between TMCs which have paramagnetic 'cores', the spatial coupling element may be scaled by a factor, $f(S_c, S)$, depending on the spin quantum number of each core (taken here as S_c for both cores) and the overall spin quantum number (S) of the DBA system (including the spin of the transferring electron, assumed to be 'high-spin' coupled to each core spin) [50,51],

$$f(S_c, S) \propto \{(2S+1)^2/2(2S_c+1)(2S_c+2)\}^{1/2} \tag{21}$$

Thus, an appreciable increase in κ_{el} (and hence degree of adiabaticity) may occur as S increases from its low spin to high spin limits (we neglect in Eq. (21), any consequences of orbital spatial anisotropy).

2.3.3. Spin–orbit coupling

In cases where thermal ET is found to require spin–orbit coupling, as for example, in the case of $Co(NH_3)^{2+/3+}$ exchange [12], the spatial matrix element may be appreciably attenuated by a factor reflecting the degree of spin–orbit coupling between the ground spin-state and the higher energy spin state required for facile ET. Spin–orbit coupling of this type may be essential even in cases where the overall ET process would remain formally spin–allowed if the spin–orbit coupling were neglected [12].

Finally, we note that in more general treatments of k_{ET}, the consequences of nuclear quantum effects are included in terms of vibronic coupling elements, in which the electronic elements (H_{if}) are scaled by nuclear Franck–Condon factors ($S_{FC} \leq 1$), thus increasing the degree of non-adiabatic character [38,42].

2.4. Coordinate dependence of the kinetic parameters

In the foregoing treatment, the ET process has been cast in terms of progress along the reaction coordinate, η (Section 2.1). The ET dynamics may be appreciably influenced by other coordinates of the system, leading to parametric dependence of k_{ET} on such coordinates and thus requiring configurational averaging if the coordinates fluctuate to a significant degree. This may occur for intramolecular as well as the case of bimolecular ET between TMCs noted in Section 2.2. The details of the configurational averaging depend on the relative time-scales and may lead, for example, to limiting cases such as homogeneous (dynamically-averaged) or inhomogeneous (statically-averaged) kinetics [38]. Coordinate induced fluctuations in H_{if} constitute departures from the Condon approximation introduced above.

Of particular importance is the effective D/A separation distance, r_{DA}, discussed further in Section 3, which influences the activation energy $G^{\dagger}$ [34] through coulombic terms ($\propto r_{DA}^{-1}$) in λ_s and ΔG°, and the coupling element, H_{if}, through exponentially varying orbital overlap [36]. Torsional modes in DBA can also modulate H_{if}. appreciably [4]. The variation of H_{if} with r_{DA} may often be expressed to good approximation as

$$(H_{if})^2 \propto \exp(-\beta r_{DA}) \tag{22}$$

a relationship especially useful for comparisons of coupling strength in a homologous family of bridges, B. The square of H_{if} is used in Eq. (22), so as to correspond to the form of the prefactor of k_{ET}^{na} (Eqs. (14)–(16)). One may also attempt to fit the r_{DA}-dependence of the overall rate constant using the exponential form of Eq. (22). If $G^{\dagger}$ has its own appreciable r_{DA}-dependence (generally, for $r_{DA} \lesssim 10$ Å), such a fit may yield an effective decay coefficient β departing appreciably from the β coefficient governing H_{if} (Eq. (22)); e.g. see [52,53].

In long-range ET, the r_{DA}-dependence of k_{ET} may be influenced by inelastic tunnelling associated with H_{if} modulation due to coordinate fluctuations [10b].

2.5. Beyond the TST framework

The kinetic model sketched in Sections 2.1–2.4 is based on simple TST in the TSA, in which the activated ET proceeds from D to A with no significant intermediate residence time of the transferring charge on the intervening bridge, and in which the dynamics of the activation process is fast relative to the timescale of the ET step in the TS (e.g. as governed by κ_{el} in Eq. (13)). In the adiabatic limit ($\kappa_{el} \sim 1$) the timescales may be reversed. In such a case, the rate determining step occurs in the activation process, leading to a kinetic regime outside of the TST framework, as in the case of solvent dynamical control of ET [38,42]. Other rate determining steps such as conformational 'gating' may also require an extension of the simple TST framework [54,55]. In kinetics beyond the TST regime, effective nuclear frequencies may be defined which are quite distinct from the TST ν_n introduced in Eq. (6) [4,38].

When intermediate bridge sites are energetically accessible to the transferring electron, the overall D→A ET kinetic process may be recast as a series of sequential diffusive hops involving such sites, and the resulting distance-dependence of k_{ET} becomes much weaker than exponential [56] (cf. Eq. (22) and associated comments).

3. Formulation of electronic states and coupling elements

The ET kinetic models presented in Section 2 were based on the two-state framework in which the electronic space is spanned by two diabatic wavefunctions, ψ_i and ψ_f, or alternatively, the adiabatic electronic states, ψ_1 and ψ_2 [57]. We now require a specification of these states and associated properties in a form capable of detailed implementation using the techniques of computational quantum chemistry, at either the ab initio or semiempirical level. It is often convenient to express the desired diabatic quantities in terms of the corresponding adiabatic quantities.

3.1. Resonant D and A sites

At the TS for thermal ET we may assume that ψ_1 and ψ_2 are 50–50 mixtures of the resonant charge-localized reactant and product states in the TSA,

$$\psi_1 = (\psi_i + \psi_f)/\sqrt{2(1+S_{if})}$$

$$\psi_2 = (\psi_i - \psi_f)/\sqrt{2(1-S_{if})} \quad (23)$$

where $S_{if} \equiv \int \psi_i \psi_f d\tau$ is the diabatic overlap integral. By construction, ψ_i and ψ_f are generally defined to be orthogonal ($S_{if} = 0$), so that by inversion of Eq. (23) we obtain

$$\psi_i = (\psi_1 + \psi_2)/\sqrt{2}$$

$$\psi_f = (\psi_1 - \psi_2)/\sqrt{2} \quad (24)$$

This relationship is enforced by symmetry for symmetric exchange. In cases where formal symmetry does not pertain, the 50–50 'resonance' is achieved (where diabatic energies H_{ii} and H_{ff} are equal) by locating the value of η where ΔE_{12} is minimized (e.g. by imposition of a suitable external perturbation) [4,17,36].

Eq. (18), relating the diabatic coupling H_{if} and the adiabatic energy gap follows directly from Eq. (24), since for energy eigenstates, $H_{12} = 0$ and

$$H_{if} = \Delta E_{12}/2 = (H_{22} - H_{11})/2 \quad (25)$$

where

$$H_{jk} \equiv \int \psi_j H_{el} \psi_k d\tau$$

(for a discussion of sign conventions see Ref. [36]). Evaluation of H_{if} via Eqs. (6) and (24) may be based on ψ_1 and ψ_2 obtained for a given DBA system at several levels of sophistication, including (1) open shell self consistent field (SCF) calculations; (2) Koopmans' theorem (KT) approximations to the direct SCF results; and (3) multiconfigurational (MCSCF) or other types of configuration interaction (CI) calculations [4,17,36]. An additional approach, found to be very effective for cases of relatively weak electronic coupling, is to obtain ψ_i and ψ_f directly from charge-localized symmetry broken (in the case of symmetry equivalent D and A sites) SCF or MCSCF calculations [36,58]. In this case, non-orthogonality ($S_{if} \neq 0$) requires an extension of Eqs. (18) and (25), yielding

$$H_{if} = \Delta E_{12}/2 = (H_{if} - S_{if}\bar{H})/(1 - S_{if}^2) \quad (26)$$

where $\bar{H} \equiv H_{ii} = H_{ff}$ at resonance.

3.1.1. Superexchange pathway analysis

The overall bridge-mediated D/A coupling implicit in H_{if} may often be usefully analyzed in terms of the superexchange (se) model [36,59,60]. Within the resonant TSA, H_{if} is decomposed into pathways defined in

terms of an auxiliary basis of zeroth-order states (or orbitals) localized on various sites of the DBA system [4,36]. Decisions as to the optimal choice for such local states to be included on each site are governed by tradeoffs between chemical interpretive convenience and computational efficiency. The coupling H_{if} is then displayed as a superposition of 'pathway' contributions [60–64], where each pathway defines a sequence of virtual steps by which the transferring charge tunnels from D and A via the selected localized bridge states. The simplest example of the se model is the perturbative expression derived by McConnell, which represents H_{if} as a single nearest-neighbor (NN, sometimes denoted as 'tight binding') pathway involving n bridge sites, with one state per site [59],

$$H_{if} = T_{D1}\left(\prod_{j=1}^{n-1} t_{j\,j+1}/\Delta_j\right)(T_{nA}/\Delta_n) \tag{27}$$

where the T and t denote NN transfer (or 'hopping') integrals, and Δ_j denotes the vertical gap separating the energies of the jth bridge state and the resonant D/A sites (perturbation theory imposes the restrictions, $|T/\Delta|$ and $|t/\Delta| \ll 1$). For homologous bridges (T, t and Δ independent of site), Eq. (27) is seen to yield the pure exponential behavior introduced in Eq. (22). Eq. (27) and its multi-path generalizations have been used extensively in analyzing and interpreting ET data obtained from both experiment and computation [4]. Superposition of pathways, as for example in the parallel occurrence of ET and HT (as well as additional 'hybrid') transfer, open the possibility of significant interference (either constructive or destructive) in the overall H_{if} [63]. Competing ET and HT for a model binuclear TMC are displayed schematically in Fig. 4 for the case $n = 2$. As the gap separating D/A and B levels is reduced, thermal occupation of charge-localized bridge sites may become significant, as noted in Section 2.5. In such a case, a sequential hopping mechanism may pertain, and se electron tunnelling between D and A sites is no longer mechanistically relevant [4,56,65]. As the bridge and D/A levels approach resonance, all states

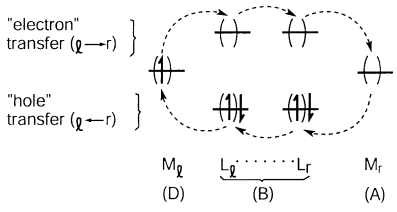

Fig. 4. Schematic orbital representation of bridge-mediated superexchange of the 'electron' (top, left to right) and 'hole' (bottom, right to left) type, illustrated for the case of intermolecular ET between two metal/ligand (M/L) complexes, where $D \equiv M_l$, $B \equiv L_l \ldots L_r$, and $A \equiv M_r$. The virtual intermediate states for the hole and electron processes involve, respectively, charge-localization in the filled ('valence') and empty ('conduction') bands of the bridge.

of the DBA system will tend to become delocalized. This type of resonance is, of course, quite distinct from resonance between D and A levels, the main focus of this subsection.

In the se model, cast in terms of the localized auxiliary states noted above, the zeroth-order D and A orbitals have their 'tails' enhanced by se mixing with the bridge states, and it is these modified D and A orbitals which define the overall coupling element H_{if} in the TSA [4,60,63].

Since the energy gaps arising in the se model (e.g. the Δ_j in Eq. (27)) involve charge transfer steps, they may be expected to be sensitive to the presence of solvent in the environment of the DBA species. In fact, such sensitivity is often found to be rather small [4,19,24,63], an outcome probably due in part to interference among many different se pathways, which would tend to yield some cancellation of solvent effects.

3.2. Non-resonant D and A sites

It is desirable to have a means of defining diabatic states (ψ_i and ψ_f) and H_{if} which is free of the constraint of D/A resonance. Thus, in the case of optical ET (Fig. 1), it is of great importance to obtain estimates of H_{if} which may be compared with corresponding values of H_{if} inferred from thermal kinetics, and which may be of value in predicting thermal kinetics when thermal H_{if} estimates are not available [4,45,66–70]. Freedom from the constraint of D/A resonance is also important from a practical point of view when it comes to computational techniques for defining and dealing with diabatic states [4].

3.2.1. The generalized Mulliken Hush (GMH) model

We now seek a formal definition of diabatic states for the general case of non resonant D and A sites. We achieve this goal by exploiting the relationship between the charge-localized, non-stationary diabatic states of a given system and the corresponding adiabatic states (spectroscopic eigenstates), which involve some degree of delocalization of the transferring charge. In Section 3.1 this relationship was considered only for the resonant situation, and for an electronic space limited to two adiabatic states, ψ_1 and ψ_2. At the outset, one may relax this latter restriction. Viewing the adiabatic states as a basis set, it is necessary to ascertain the smallest set capable of adequately representing the desired diabatic states, ψ_i and ψ_f. To proceed further we adopt the generalized Mulliken Hush (GMH) criterion for defining the diabatic states, i.e. those which exhibit the maximum degree of charge localization [4,63,71]. According to this criterion, for any given space of electronic states (defined in terms of a set of n adiabatic states), the diabatic states are those which diagonalize the projection of the electronic dipole

moment vector operator ($\hat{\mu}$) in the direction of the charge transfer process, and hence maximize the differences among the state dipole moments (projected on the same reference direction). When $n > 2$, one obtains additional diabatic states as well as the primary D/A pair. In the traditional Mulliken–Hush (MH) approach [72] it is assumed that a two-state adiabatic space (ψ_1 and ψ_2) is adequate for representing ψ_i and ψ_f. Further perspective on definition of diabatic states is given in Ref. [73] and in the previous literature cited in Ref. [71].

Adopting a two-state diabatic basis and the above criterion for defining diabatic states, together with the assumption that ψ_i and ψ_f are orthonormal, and the identification of the reference charge transfer direction as that defined by the adiabatic dipole moment shift,

$$\Delta\hat{\mu}_{12} \equiv \hat{\mu}_{22} - \hat{\mu}_{11} \tag{28}$$

where $\hat{\mu}_{ij} \equiv \int \psi_i \hat{\mu} \psi_j d\tau$ leads to the following expression for D/A coupling according to the GMH model

$$|H_{if}| = \mu_{12}\Delta E_{12}/\Delta\mu_{if}| \tag{29}$$

where

$$\Delta\mu_{if} = ((\Delta\mu_{12})^2 + 4(\Delta\mu_{12})^2)^{1/2} \tag{30}$$

Here ΔE_{12} is the vertical adiabatic energy gap (the vertical separation of the two-state energy eigenvalues introduced in Eq. (18) for the special case of resonant D and A sites). The natural definition of the effective D/A separation, r_{DA}, now becomes [71],

$$r_{DA} \equiv \Delta\mu_{if}/e \tag{31}$$

where e is the magnitude of the electronic charge. In the case of symmetrically delocalized adiabatic states, which are composed of 50–50 mixtures of resonant diabatic states, Eq. (29) is seen to yield Eq. (18).

A great advantage of the GMH model (Eqs. (29) and (30)) is that it can be applied to an arbitrary nonresonant situation. Of course, in some cases it may be necessary to relax the constraints of the two-state adiabatic model [71]. Eqs. (29) and (30) show that H_{if} and r_{DA} may be determined entirely on the basis of spectroscopic (i.e. adiabatic state) information, whether from experiment (optical transition energies, oscillator strengths, and dipole shifts from Stark data) or from quantum calculations (SCF or CI). In contrast to the earlier MH model [72], Eqs. (30) and (31) reveal that the two-state model implies a value for the effective D/A separation, r_{DA}, without requiring the use of independent assumptions.

In summary, thermal and optical processes are seen to give complementary accounts of the underlying D/A interaction. This is especially transparent for the case of a two-state space where Eq. (29) shows explicitly how the diabatic Hamiltonian matrix element, governing the magnitude of the thermal ET rate constant is related to the adiabatic dipole matrix element (the transition dipole), governing the intensity of the corresponding optical ET process (see Fig. 1).

It has been found that in some cases, H_{if} magnitudes obtained from optical data via Eq. (29) seem to be underestimated in comparison with independent estimates of H_{DA} from thermochemical data [67,68]. Such discrepancies may be due to the use of inappropriate estimates of r_{DA} (e.g. using assumed values based on molecular coordinates instead of Eq. (31)) or from inadequacies of the two-state model. In any case, ambiguities pertain in general to all models for estimating H_{if} magnitudes. In the remainder of the present study we employ the two-state GMH model, and where contact with experiment is possible, reasonable agreement is generally found [4]. In cases of quasidegeneracy within initial or final state manifolds, where the overall electronic space involves more than two states, or other situations where alternative candidate for ψ_i and ψ_f may arise, it is nevertheless often found that viable two-state subspaces may be identified, as discussed further below. When it is deemed necessary to employ a larger state space ($n > 2$), one must evaluate the limitations of the purely electronic framework for coupling adopted here, in comparison with a more general vibronic formulation [74,75].

Finally, we note that the superexchange model introduced in Section 3.1 for the resonant D/A case (Eq. (27)) can be extended to nonresonant situations, using an appropriate definition of effective energy gap Δ [36,66].

4. Computational applications and comparisons with experiment

We survey here the results of calculations of electronic coupling elements (H_{if}) and activation energetics for a broad range of ET systems of the DBA type, involving both bimolecular and intramolecular, and thermal and optical processes (recall the generic sense in which 'bridge' (B) was introduced in Section 2 so as to accommodate a variety of situations without necessarily implying a formal covalent linkage of D and A sites). The calculated results are analyzed in terms of the theoretical constructs presented in Sections 2 and 3, and in a number of cases, detailed comparison is made between calculated and experimental results.

The theoretical calculations were based for the most part on semiempirical (INDO) quantum chemical electronic structure calculations, and in one case (Section 4.3), on large-scale molecular dynamics (MD) simulations [14]. The version of the INDO method used here is that based on the 'spectroscopic' Hamiltonian (INDO/s) parameterized by Zerner and coworkers for systems including both organic and transition-metal based moieties [76], and is thus especially effective in treating

electronic properties of TMCs, including evaluation of H_{if} [4,36]. On the other hand, the method is not parameterized for calculating features of potential energy surfaces, so that necessary bond lengths and force constants needed in modeling ET kinetics must be obtained from independent sources. Given our particular focus on H_{if}, it is notable that in several cases where comparison has been made, INDO/s results for H_{if} are found typically to be within $\sim$25% of ab initio SCF results, as indicated by the results for model electron exchange processes in Table 1 [77] (see also [64]).

The remainder of this section focusses on the role of metal/ligand (ML) mixing in controlling H_{if} magnitudes (Section 4.1), issues related to alternative choices of initial and final states in ET processes and the consequences for H_{if} (Section 4.2), and finally detailed analysis of activation energetics (Section 4.3).

4.1. Role of metal/ligand (ML) mixing

While ET between TMCs may often be viewed nominally as metal-to-metal charge transfer (MMCT), it is clear that the actual contact between the TMCs (whether in a bimolecular process or in a binuclear complex) is to a significant extent established by the ligands [13,19,36,60,78,79]. Hence the effectiveness of the overall MM electronic coupling (manifested in H_{if}) depends crucially on the extent to which the transferring charge is partially delocalized onto the ligands, both in the initial (ψ_i) and final (ψ_f) states at the TS. This will be true whether the ligands are in direct contact (as in encounter complexes in bimolecular ET between TMCs with single coordination shells), or indirectly, as mediated by tethers. The specific examples considered In Sections 4.1.1 and 4.1.2 involve bimolecular ET processes.

The influence of ML mixing on H_{if} can be cast in terms of superexchange theory (Section 3.1.1), as illustrated in Fig. 4, where the collective bridge (B) is represented by a pair of ligands ($n=2$) in contact. The relative importance of electron (ET) and hole (HT) transfer is then controlled by the ML hopping integrals (T, in Eq. (27)) and, respectively, the energy gaps for metal-to-ligand (MLCT) and ligand-to-metal (LMCT) charge transfer (another transfer integral, the ligand–ligand coupling element t (see Eq. (27)), is needed to 'complete the circuit') [13].

For a binuclear TMC system, one may employ a simpler se model based on a single bridge site ($n=1$ in Eq. (27)), yielding the following superposition of ET and HT pathways, developed specifically for ET involving low-spin Ru^{2+} and Ru^{3+} sites [4,66,69],

$$H_{if} = \frac{T_{ML}T_{M'L}}{2\Delta E_{ML}} + \frac{T_{LM'}T_{LM}}{\Delta E_{LM}} \quad (32)$$

where ML (M′L) and LM (LM′) refer, respectively, to MLCT and LMCT processes, and ΔE_{ML} and ΔE_{LM} are effective MLCT and LMCT energy gaps [36,66]. Eq. (32) has been used with reasonable success [66,69] to correlate optical data for MLCT and LMCT (right hand side) with H_{if} estimates based on optical data for MMCT (left hand side), also known as the intervalence transition (IT). The extent of ML mixing is reflected in effective D/A separation distances (r_{DA}) inferred from experimental optical data using the definition provided by GMH model (Eqs. (30) and (31)), as illustrated in Table 2 (see also Ref. [5]). The r_{DA} values are appreciably less than the nominal values based on molecular structure (metal sites and ligand midpoints), and the spectroscopic value can be significantly smaller than the diabatic value (based, respectively, on $\Delta\mu_{12}$ and $\Delta\mu_{if}$).

4.1.1. Electronically saturated ligands

Water and ammonia are familiar examples of electronically saturated ligands which lack low-lying orbitals

Table 1
Calculated H_{if} values for $ML_n^{2+/3+}$ self exchange ($n=1$ or 3): ab initio vs. INDO/s results[a]

M	L	Transfer type[b,c]	r_{MM} (Å)	H_{if} (cm^{-1})			
				Ab initio		INDO/s	
				Deloc[d]	Loc[e]	Deloc[d]	Loc[e]
Co	NH_3	σ (A–A)	7.0	1400	2820	1740 (+24%)[f]	3455 (+23%)
Fe	H_2O	σ (A–A)	7.3	408	312	308 (−24%)	279 (−11%)
Fe	H_2O	π (A–A)	7.3	26	27	32 (+23%)	30 (+11%)
Fe	H_2O	σ (F–F)	5.3	146	110	108 (−26%)	87 (−21%)

[a] Table 1 of Ref. [77], reprinted with kind permission. Copyright 1992, Plenum Press.
[b] Symmetry of D and A orbitals with respect to the MM axis.
[c] A–A ≡ apex–apex ($n=1$); F–F ≡ face–face ($n=3$).
[d] Based on adiabatic state splitting, ΔE_{12} (Eq. (18)).
[e] Based on charge-localized (symmetry-broken) SCF wavefunctions.
[f] Percent deviation of INDO/s result relative to ab initio result.

and hence are expected to serve as electron donors, thus leading to dominance of the HT se pathway (via LMCT) in establishing the magnitude of H_{if} [36]. Analysis of detailed ab initio calculations for electron exchange in some model aquo and ammine $Fe^{2+/3+}$, $Ru^{2+/3+}$, and $Co^{2+/3+}$ complexes with a common linear ML···LM geometry, yielded proportionality between H_{if} and the square of the ML covalency parameter, thus underscoring in a compact, quantitative manner the nature of ligand-mediated overall M–M coupling in these systems [78]. On the other hand, H_{if} magnitudes for complexes of a given ML_6 type can depend strongly on the relative orientation of the TMC in the bimolecular TS. This is illustrated in Table 3, on the basis of INDO/s SCF results [36]. In the case of the relatively 'intimate' face-to-face (F–F) approach geometry, intermolecular L···M (and perhaps even M···M) contacts may be significant in addition to the pathway involving L···L contact. Such dominant orientation dependence precludes any simple variation of H_{if} with r_{DA} (of the type expected for homologous DBA systems (Eq. (22)) if comparisons are made among systems with different orientations.

Table 3
Calculated dependence of H_{if} on encounter geometry in bimolecular electron exchange[a]

Orientation[b]	H_{if} (cm^{-1})[c]	r_{MM} (Å)[d]
π-Electron exchange[e]*: $Fe(H_2O)_6^{2+/3+}$*		
Face-to-face	40	5.3
Edge-to-edge	21	6.4
Apex-to-apex	17	7.4
σ-Electron exchange[f]*: $Co(NH_3)_6^{2+/3+}$*		
Face-to-face	74	5.8
Edge-to-edge	120	6.9
Apex-to-apex	580	7.0

[a] Table V of Ref. [36], reprinted with kind permission. Copyright 1991, American Chemical Society.
[b] The three indicated orientations correspond to approach geometries in which the two octahedral reactants, have, respectively, a common three, two and fourfold axis.
[c] The H_{if} are obtained from calculated splittings (Eq. (18)) based on restricted Hartree–Fock (RHF) INDO/s SCF wavefunctions for the $[(ML_6)(ML_6)]^{5+}$ supermolecule complex.
[d] Metal–Metal separations for reactants at van der Waals contact for each orientation.
[e] Exchange of a t_{2g}-type electron.
[f] Exchange of an e_g-type electron, based on low-spin states of Co^{2+} (^2E_g) and Co^{3+} ($^1A_{1g}$)

4.1.2. Metallocene-based ET systems

For exchange between ferrocene/ferrocenium (Fc/Fc^+) or the cobalt analog (Cc/Cc^+, where Cc denotes cobaltocene), the unsaturated cyclopentadienyl (Cp) ligand can serve as an electron donor (LMCT), but also an acceptor (via a somewhat higher energy MLCT process) [13,76]. Thus, the relative importance of ET and HT pathways for H_{if} is not immediately obvious. Group theory and analysis of INDO/s results for H_{if} suggest that ET and HT are, respectively, the dominant se pathways for the ferrocene and cobaltocene exchange processes. Using quasi cylindrical symmetry, we find that the transferring charge for Fc and Cc resides in orbitals, respectively, of $\delta(3d_{x^2-y^2}$ or $3d_{xy})$ and $\pi(3d_{xz}$ or $3d_{yz})$ symmetry (where z is the cylindrical axis), while the highest occupied and lowest unoccupied orbitals of Cp are, respectively, of π and δ symmetry. Hence the LMCT pathway (the one with the lower energy gap) does not couple to the transferring electron on Fc, leaving the higher energy ET pathway (via MLCT) as the symmetry-allowed route for H_{if} [13].

Table 2
Effective separation of D/A sites (r_{DA} (Å))

ET system		From molecular geometry[a]	From two-state analysis of spectral data[b]	
			Diabatic	Adiabatic
$(NH_3)_5(Ru^{2+}L)$[c]				
MLCT[d]	L = pz	3.5	2.2	1.0
	L = pzH^+	3.5	2.1	< 0.1
	L = bpy	5.6	3.4	2.9
	L = $bpyH^+$	5.6	4.3	3.6
$(NH_3)_5(Ru^{2+}LRu^{3+})NH_3)_5$[c]				
IT[e]	L = pz	6.8	1.4	< 0.1
	L = bpy	11.3	5.2	5.1

[a] Based on separation of M and ligand midpoint (for MLCT cases) or $r_{MM'}$ (for IT cases), where M and M′ denote Ru atom sites. (Table 2 of Ref. [4], reprinted with kind permission. Copyright 2001, Wiley–VCH.)
[b] Based on spectral data analyzed in terms of the two-state GMH model (Eq. (29)). In the analysis a value of $f = 1.3$ was used to relate the local to the applied external electric field in the Stark measurements ($\vec{E}_{loc} = f\vec{E}_{ext}$).
[c] Refs. [5,98,99]; pz ≡ pyrazine; bpy ≡ 4,4-bipyridine.
[d] MLCT ≡ metal-to-ligand charge transfer.
[e] IT ≡ intervalence transfer.

Comparison of calculated [13] and experimental [80] H_{if} estimates is provided in Table 4, showing that the calculated results based on the lowest energy encounter complexes (separated by ≥ 3 kcal mol^{-1} from other structures [13]) bracket the experimental values. The results for Cc imply the adiabatic ET regime ($\kappa_{el} \sim 1$), whereas Fc appears to be near the non-adiabatic/adiabatic boundary.

Further comparison between calculation and experiment is provided in Table 5 for intramolecular ET between Fc and Fc^+ sites linked by an acetylenic (A) or an ethylenic (E) group, in DBA structures denoted, respectively, as $(FcAFc)^+$ and $(FcEFc)^+$ [81–83]. Here, aside from a single CH_3O-substituent on each Fc in the $(FcAFc)^+$ system studied experimentally [82], the chemical structures used in the calculations [81] and in the experiments [82,83] are the same. The calculated and experiment results are in basic agreement. There is, however, an ambiguity regarding the conformation of the Fc groups with respect to the bridges in the systems studied experimentally (*trans* and *cis* limiting conformations were considered). The calculated results show two different trends: H_{if} (A) > H_{if} (E) for the *trans* conformation (by $\sim 20\%$), and H_{if} (*trans*) > H_{if} (*cis*) for A, but only by 5%. The experimental data was analyzed in terms of the original MH model [72] using the spectroscopic values of ΔE_{12} and μ_{12}, with r_{DA} estimated as r_{FeFe} based on structural models for the *cis* and *trans* isomers. The calculations for $(FcAFc)^+$ indicate that μ_{12} and $\Delta\mu_{if}$ (and hence r_{DA}) have very similar *trans*/*cis* ratios, with the overall *trans*/*cis* H_{if} ratio corresponding to the *trans*/*cis* ratio of ΔE_{12} values (1.05). Hence the calculated H_{if} (*trans*) slightly exceeds H_{DA} (*cis*), even though the r_{DA} values by themselves (via Eq. (30)) yield a ratio less than unity (0.9).

Table 5
Comparison of calculated and experimental H_{if} values for $(FcAFc)^+$ and $(FcEFc)^+$ [a]

System	r_{FeFe} (Å) [b]	H_{if} (cm^{-1})	
		Calculated [c]	Experiment [d]
$(FcAFc)^+$	6.4 (*cis*)	649 (*cis*)	525 (*cis*) [e]
	7.3 (*trans*)	682 (*trans*)	427 (*trans*) [d]
$(FcEFc)^+$	6.2 (*cis*)	589 (*cis*)	559 (*cis*) [f]
		492 (*trans*) [f]	492 (*trans*) [f]

[a] Adapted from Table III of Ref. [81], reprinted with kind permission. Copyright 2002, American Chemical Society. The Fc groups are linked by actylenic (A) or ethylenic (E) bridges.
[b] Values for the structures used in the calculations [13].
[c] Based on the GMH model [71], Eqs. (29) and (30).
[d] Based on the MH model [72], taking r_{DA} as the r_{FeFe} estimates for *cis* and *trans* isomers.
[e] Ref. [82]; results based on acetonitrile solvent; *cis* and *trans* r_{FeFe} values taken as 5.85 and 7.20 Å, respectively.
[f] Ref. [83]; results based on dichloromethane solvent; *cis* and *trans* r_{FeFe} values taken as 6.19 and 7.03 Å.

4.2. Alternative initial and final states

Implementation of the TSA becomes ambiguous in cases of near degeneracy [13,17,25,45,76,81,84] (common in open shell TMCs, where for example, perturbation of idealized octahedral symmetry may lead to splitting of t_{2g} and e_g states), or other situations where the appropriate choice of ψ_i and ψ_f is not obvious [12,14,85]. The choice in general involves a tradeoff including thermal access (in the case of initial states), and the state-dependence of activation energy ($G^\dagger$) and coupling (H_{if}) [12,14].

4.2.1. Near-degeneracy

In cases of near-degeneracy in D or A manifolds, typically one may find that one component state couples effectively to the bridge (hopping integral T in Eq. (27)), while the other component couples weakly due to the nodal structure of the D or A orbital. An example is provided in Table 6 for the case of Fc and Fc^+ linked by unsaturated bridges of the type 'APA' and 'VPV', where A, E and P denote, respectively, an acetyenic, an, ethylenic, and a *p*-phenylenic moiety [81] (see Fig. 5). In the isolated ferrocene molecule the $3d_{x^2-y^2}$ and $3d_{xy}$ orbitals (and hole states) are degenerate, but due to different orientation of nodal planes in the tethered DBA systems, $3d_{x^2-y^2}$ (which overlaps with a Cp molecular orbital (MO) having a finite contribution at the carbon atom linked to the bridge) lies above the $3d_{xy}$

Table 4
Calculated and experimental estimates of H_{if} (cm^{-1}) for $(CpFeCp)^{o/+}$ and $(CpCoCp)^{o/+}$ [13]

Encounter geometry [a]	Intermolecular contact [b]		Fe(δ) [c]		Co(π) [c]	
	r_{MM}	r_{CC}	Calc.	Exp. [d]	Calc.	Exp. [d]
Coaxial (D_{5h})	6.75	3.39	135	35	920	175
T-shaped (C_s)	6.50	3.63	99		70	

[a] Lowest-energy structures [13].
[b] Metal–metal and shortest bimolecular carbon–carbon contact distances (Å).
[c] Symmetry-type of D and A orbitals, based on psudo cylindrical symmetry.
[d] Ref. [80].

Table 6
Quasi degenerate hole states in $(FcAPA\ Fc)^+$ and $(Fc\ EPEFc)^+$ [a]

Fe 3d-hole type[b]		H_{if} (cm^{-1})	Relative energy (eV)[c]
$(FcAPAFc)^+$	$3d_{x^2-y^2}$	177	0.000
	$3d_{xy}$	2	0.058
$(FcEPEFc)^+$	$3d_{x^2-y^2}$	140	0.000
	$3d_{xy}$	0.4	0.051

[a] Table IV of Ref. [81], reprinted with kind permission. Copyright 2002, American Chemical Society. The APA and EPE bridges are defined in Fig. 5.

[b] Dominant character of calculated hole state, where z is the Fc axis and the x axis is aligned with the single bonds linking the Fc Cp rings to the bridge. In the $3d_{xy}$-hole states, the hole resides predominantly in an Fe orbital which mixes with Cp molecular orbitals bearing a node on the carbon atom linked to the bridge, thus accounting for the very small H_{if} magnitudes.

[c] Based on INDO/s SCF/CI calculations.

orbital (which has a node at the linked Cp carbon atom). Thus the hole ground states ($3d_{x^2-y^2}$) are the ones which yield good overall D/A coupling, as displayed in Table 6. Nevertheless, the $3d_{xy}$ hole states, which yield very small coupling ($|H_{if}| \lesssim 1\ cm^{-1}$), are calculated to lie only 0.05–0.06 eV higher and thus are thermally accessible at room temperature. The relative occupations of the two hole states could of course be altered by suitable chemical substituents on the Cp rings.

Michl and coworkers have discussed the potential role of $(C_4R_4)Co(C_5H_5)$ complexes (Fig. 6) in conductive two-dimensional assemblies, in which the cyclobutadiene rings may be linked via suitable substituents R [86]. Denoting the complex as CbCoCp, where R = H for the present discussion, we note that it may be viewed as basically isoelectronic (as far as the relevant Co and ligand MOs are concerned) with ferrocene (CpFeCp), with nominal group oxidation states Cb^{2-} Co^{3+} Cp^-, in contrast to Cp^- Fe^{2+} Cp^-. In Table 7 we compare the low-lying hole states of CbCoCp and CpFeCp, based on INDO/s open-shell restricted Hartree–Fock calculations [81]. The primary feature of interest is the relative order of the non-degenerate $3d_{x^2-y^2}$ and $3d_{xy}$ hole states in $(CbCoCp)^+$. While the overall symmetry

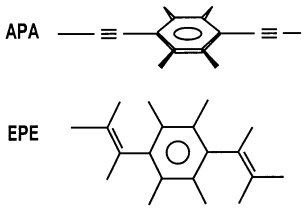

Fig. 5. Schematic representation of the 'APA' and 'EPE' spacers, comprised of acetylenic (A), phenylene (P), and ethylenic (E) moieties. The A and E labels are used as convenient substitutes for standard organic nomenclature (respectively, ethynylene and vinylene). In the calculations, the EPE framework was kept planar, and the attached cyclopentadienyl ferrocene ligands in the full DBA systems for both APE and EPE were coplanar with the phenylene groups.

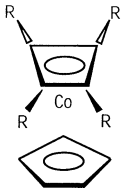

Fig. 6. Cyclobutadiene (R = H)/cyclopentadiene Co sandwich complex (isoelectronic with ferrocene as far as relevant valence molecular orbitals are concerned).

of the CbCoCp structure can be at most C_s, the local C_{4v} symmetry of the CbCo moiety plays an important role, with the anitbonding Cb pi MO (b_1) mixing with the Co $3d_{x^2-y^2}$ orbital and pushing it below the $3d_{xy}$ orbital (b_2), whose nodal planes contain the Cb carbon atoms and thus in the local C_{4v} symmetry do not mix with any of the Cb pi MOs. This simple orbital argument can explain qualitatively why the ground hole state is $3d_{xy}$ [81,87]. This result has implications for electronic coupling when CbCoCp units are linked, since as discussed above, the $3d_{xy}$ orbitals yield much less favorable coupling than the $3d_{x^2-y^2}$ orbitals. On the other hand, covalent coupling to a bridge will tend to raise the $3d_{x^2-y^2}$ energy level relative to that for $3d_{xy}$ (as happens when tethers break the $3d_{x^2-y^2}/3d_{xy}$ degeneracy in the case of Fc-based DBA systems [81]). Substituents (R) on the Cb ring will also have a bearing on the relative $d_{x^2-y^2}$ and d_{xy} energy levels.

Other examples of near-degeneracy effects pertain to ET involving low-spin $Fe^{2+/3+}$ and $Ru^{2+/3+}$ couples complexed to aza aromatic ligands. The case of tris bipyridyl (bpy) Fe^{2+} and Fe^{3+} sites linked by three polymethylene chains ($(CH_2)_m$) with approximate C_3 symmetry (schematically represented by structure **1**(m)) is especially interesting [45]. While the low spin t_{2g} states of the Fe^{3+} site are split into ground (^2A) and excited

Table 7
Comparison of low-lying hole states for ferrocene and $(C_4H_4)Co(C_5H_5)$[a]

	Hole state[c]	Relative energy (eV)[d]
Ferrocene	$3d_{x^2-y^2}$, $3d_{xy}$	0.00
	$3d_{z^2}$	0.48
$(C_4H_4)Co(C_5H_5)$[b]	$3d_{xy}$	0.00
	$3d_{z^2}$	0.27
	$3d_{x^2-y^2}$	0.33

[a] Adapted from Table VI of Ref. [81], reprinted with kind permission. Copyright 2002, American Chemical Society.

[b] Structure given in Fig. 6 (R = H).

[c] The 3d-type hole states are based on a coordinate system where the z axis is perpendicular to the ring planes and where the x and y axis are parallel to the diagonals of the C_4 ring. Thus, the C_4 carbons lie in the nodal planes of the $3d_{xy}$ orbital (cf. related comments in footnote b of Table 6).

[d] The ground and low-lying excited states were obtained from separate direct SCF calculations.

(^{2}E) states separated by only $\sim 100\ cm^{-1}$, the larger spin orbit coupling constant (estimated at $\sim 440\ cm^{-1}$) requires the use of spin–orbit adapted states in analyzing both the thermal and optical ET processes, in which a single thermally accessible initial state is significantly coupled to two separate final states, estimated to be split by $\sim 3k_BT$ at room temperature [45]. If the spin orbit coupling were absent, only the ground state ET process would have appreciable weight (i.e. that linking the ^{2}A hole states at the two Fe sites), since H_{if} for the $^2E \rightarrow {}^2E$ process would be very small, even though the thermal population of the initial ^{2}E state would be substantial.

4.2.2. High spin versus low spin states

The mechanism of ET involving the $Co^{2+/3+}(NH_3)_6$ couple requires careful consideration of the roles of high spin (hs) and low spin (ls) electronic states (see Table 8) [12,14,85]. In the absence of spin–orbit mixing, the ground state aqueous exchange process, while formally spin-allowed, would be extremely slow, since it involves a 'three-electron' process: i.e. in addition to the transfer of one electron, an additional 'shakeup' process is required at each site ($t_{2g} \rightarrow e_g$ and $e_g \rightarrow t_{2g}$ at the sites being, respectively, reduced and oxidized), so as to maintain the ground state configuration in the course of the exchange [12]. Spin–orbit mixing of the excited configurations with their ground state counterparts (Table 8) yields a 'one-electron' process (transfer of an electron between e_g orbitals at the two sites), but at the cost of a very small κ_{el} value (estimated to be $\sim 10^{-3}$ for an apex-to-apex encounter complex, and $\sim 10^{-4}$ when orientational averaging is included). On the other hand, a thermally excited purely ls mechanism has the advantage of a reduced reorganization energy (within the ls manifold) and also adiabatic behavior ($\kappa_{el} \sim 1$), which would at least partially offset the energy penalty due to the thermal excitation required to promote the system from the hs to ls manifold. In fact, detailed calculations based on both ab initio and INDO/s methods, indicate that the net tradeoff unequivocally favors the ground-state (spin–orbit-enhanced) route, as summarized in Table 9 [12]. The small κ_{el} values cited above correspond to an effective H_{if} in which a large spatial matrix element linking e_g orbitals on the two sites

Table 8
High spin and low spin states of $Co(NH_3)_6^{2+3+}$

Electronic state	Oxidation state	
	3+	2+
Ground	$^1A_{1g}$ (t_{2g}^6)	$^4T_{1g}$ ($t_{2g}^5e_g^2$)
Excited	$^3T_{1g}$ ($t_{2g}^6e_g^1$)	^2E_g ($t_{2g}^6e_g^1$)

For further details see Ref. [12]. Symmetry designations are based on O_h point group symmetry for the CoN_6 framework (lower symmetry results when account is taken of Jahn–Teller distortion [12]).

Table 9
Contributions to high spin and low spin k_{ET} ratio for $Co(NH_3)_6^{2+/3+}$ aqueous exchange: k_{ET} (ground, high spin Co^{2+})/k_{ET} (thermally excited, low spin Co^{2+})

Contribution	Factor in ratio
Activation	9.5×10^{-10}
Electronic transmission	$9.7 \times 10^{+3}$
Total	9.2×10^{-6}

Estimates based on approximate orientational averaging of reactants [12]. For a more detailed breakdown, see Ref. [12].

($\sim 600\ cm^{-1}$ for the apex-to-apex geometry) is scaled by a spin–orbit attenuation factor $\gamma^{SO} = 0.014$. We note that the estimated k_{ET} value emerging from the calculations [12] is significantly smaller than the experimental estimate (k_{ET} (calc) /k_{ET} (exp) $\lesssim 4 \times 10^{-3}$).

The qualitative features of the energetics for $Co^{2+/3+}$ exchange are shown schematically in Fig. 7a (for simplicity, diabatic profiles are sketched, whereas the adiabatic energetics were estimated in the full calculations [12]). A contrasting situation is depicted in Fig. 7b for reduction of Co^{3+} by a reduced bipyridyl ligand (bpy^-) at the Ru^{2+} site in a tethered binuclear complex [14] (see Fig. 8), dealt with in more detail in Section 4.3. Here, the preference for the ls mechanism is dominated by the more favorable κ_{el} for the ls final state (ψ_f). The spin–orbit attenuation factor γ^{SO} is expected (on the basis of the approach given in [12]) to be appreciably larger than the value of 0.014 cited above for $Co^{2+/3+}$ exchange, since the spin–orbit mixing controlling H_{if} in the former case is first-order, in contrast to the second-order mixing in the latter case. The activation free energies ($G^\dagger$) for the hs and ls processes are estimated to be comparable, due to compensating effects involving inner-shell reorganization energy and driving force ($-\Delta G^\circ$), each of which is larger for the hs process. Thus, the hs ground final state (ψ_f') is expected to be formed not directly, but rather via intersystem crossing from the initially-formed ls excited state (ψ_f). For related behavior see [85].

4.3. Calculation of activation parameters: a case study

As a final computational example, we summarize results of a recent attempt to provide a comprehensive mechanistic account of long-range et in a complex molecular solute in aqueous solution by exploiting MD and electronic structure techniques [14].

4.3.1. ET system

The DBA system is displayed in Fig. 8, consisting of a derivatized [$(bpy)_2Ru^{2+}(bpy)^-$] donor group (where bpy ≡ 2,2-bipridine), a $(pro)_4$ bridge (where pro ≡ proline and the tetrapeptide is in a polyproline II helical conformation), and a [$-O^-Co^{3+}(NH_3)_5$] acceptor

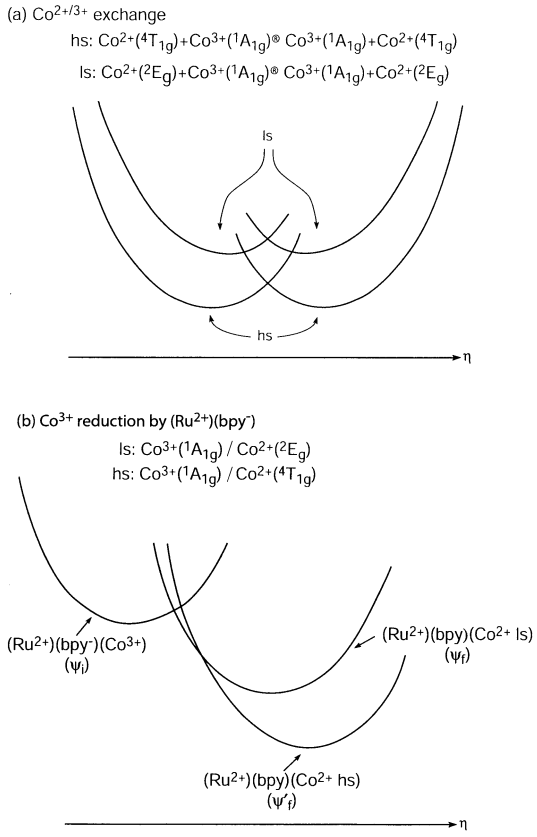

Fig. 7. Schematic depiction of energy profiles for high spin (hs) and low spin (ls) aqueous ET processes involving Co^{2+}: (a) $Co(NH_3)_6^{2+/3+}$ self exchange [12]; (b) reduction of an $(-O^-Co^{3+}(NH_3)_5)$ acceptor site by a tethered $(bpy)_2Ru^{2+}(bpy^-)$ donor site [14] (see detailed structure in Fig. 8).

group. The nominal redox process corresponds schematically to (see Fig. 7b),

$$Ru^{2+}(bpy)^-(Co^{3+}) \rightarrow Ru^{2+}(bpy)(Co^{2+}) \quad (33)$$

where the excess electron localized on the bpy linked (by a carbonyl group) to the $(pro)_4$ bridge reduces the Co^{3+} site. This system is of interest for detailed theoretical

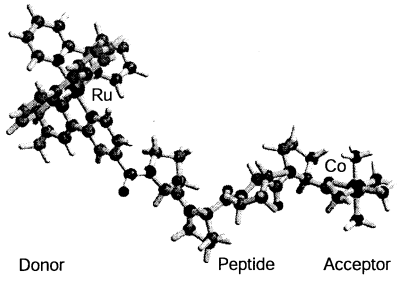

Fig. 8. Diagram of the ET system discussed in Section 4.3. The peptide bridge contains four proline residues, the donor is a derivative of $(bpy)_2Ru^{2+}$ (bpy^-) (where bpy ≡ 2,2-bipyridine, with the transferring electron in the initial state largely localized on the bpy ligand linked to the bridge), and the acceptor is $-O^-Co^{3+}(NH_3)_5$. (Fig. 1 of [14], reprinted with permission. Copyright 1995, American Chemical Society.)

study because it is a member of a homologous series for which a large body of kinetic data exists [88].

4.3.2. Mechanistic issues

Among the mechanistic issues dealt with in the full study [14] (including kinetic tradeoffs involving different Co^{2+} spin states in the reaction product and the role of solvent and conformational fluctuations of the DBA system) we focus here on the activation parameters, including nuclear tunnelling and entropy effects which are found crucial in establishing meaningful contact with the Arrhenius parameters obtained from the experimental rate data [88]. The theoretical analysis [14] also leads to new insights regarding the extent to which different thermodynamic quantities are harmonic with respect to the ET reaction coordinate.

4.3.3. Computational model

The structure and energetics pertaining to the nuclear coordinates were modeled with a Charmm-type force field for the DBA system (Fig. 8) and a T1P3P potential for ∼1000 water molecules used to represent the solvent [14,89]. Free energy and enthalpic and entropic contributions were obtained from MD simulations. Nuclear tunnelling (Section 2.2) was included via discretized path integral techniques (for the acceptor group, a major site of tunnelling) and semiclassical techniques (for the remainder of the DBA system and for the solvent) [90]. H_{if} values were obtained from GMH (Eqs. (29) and (30)) analysis of the results of INDO/s CI calculations for the DBA system. A final crucial aspect of the model arises from the fact that the reaction has a finite driving force ($-\Delta G^\circ \neq 0$). Thus in contrast to most previous simulations, which dealt with symmetric exchange reactions ($\Delta G^\circ = 0$), the model Hamiltonian for the final state of the ET process (Eq. (33)) was adjusted with a constant offset, which by construction constrained the overall calculated ΔG° at room temperature to match experimental estimates based on redox reduction potentials and spectral data (a value of $\Delta G^\circ = -13.84$ kcal mol^{-1} was adopted, based on low-spin Co^{2+} [14]). The offset does not, of course, constrain the individual enthalpy (ΔH°) and entropy (ΔS°) terms, leaving them to be determined by the detailed simulations. It is important to emphasize that in spite of the large number of empirical parameters used to define the initial and final state Hamiltonians, they are all derived from basic structural and energetic data and in no sense are fitted to kinetic data.

4.3.4. Matching of phenomenological and theoretical rate constant models

The rate constant (k_{ET}) was expressed in terms of the results of the computer simulations, using a non-adiabatic TST model (Eq. (15)). Since the experimental results were analyzed in terms of a phenomenological

Arrhenius model [88], agreement between experiment (left hand side) and theory (right hand side) would yield the following two equations. For the weakly temperature-dependent prefactor we have:

$$(k_B T/h)\exp(S'^{\dagger}/k_B) = (2\pi H_{if}^2/\hbar)(4\pi k_B T\lambda)^{1/2}\exp(S^{\dagger}/k_B) \quad (34)$$

and for the Boltzmann factor:

$$\exp(-(H^{\dagger})^{exp}/k_B T) = \exp(-(H^{\dagger})^{calc}/k_B T) \quad (35)$$

In Eq. (34), $S^{\dagger}$ is the 'true' activation entropy (see Eq. (8)). By contrast, $S^{\dagger\prime}$ is a 'pseudo' entropy of activation, which includes the contribution from the non-adiabatic prefactor (see Eqs. (14) and (15)) in addition to the quantity $S^{\dagger}$ defined in Eq. (8). Thus in order to infer the value of H_{if} from the experimental data ($S^{\dagger\prime}$), one must know the value of $S^{\dagger}$ (not directly available from the data of Ref. [88]). In Eq. (35), $(H^{\dagger})^{exp}$ is the empirical Arrhenius activation energy, and the calculated value, $(H^{\dagger})^{calc}$, is given by (see Eq. (8)),

$$H^{\dagger} = G^{\dagger} + TS^{\dagger} \quad (36)$$

4.3.5. Relationship between activation and net thermodynamic quantities

It is well known from Marcus theory that for diabatic free energies that are harmonic with respect to the reaction coordinate, $G^{\dagger}$ is a quadratic function of ΔG° (Eq. (2)) [34]. This result may be extended to H and S and represented as follows [14,91]:

$$X^{\dagger} = (1+\alpha)(\Delta X^{\circ}/2) + (1-\alpha^2)(\lambda_X/4) \quad (37)$$

where $X \equiv G$, H or S.

$$\lambda_G \equiv \lambda$$

$$\lambda_S = -\mathrm{d}\lambda/\mathrm{d}T$$

$$\lambda_H = \lambda + T\lambda_S \quad (38)$$

and where

$$\alpha \equiv \Delta G^{\circ}/\lambda \quad (39)$$

is a relative measure of the driving force (the reorganizational entropy, λ_S, should not be confused with the solvent reorganization free energy, λ_s, introduced in Section 2). Thus in the harmonic regime a knowledge of ΔX° directly yields an estimate of $X^{\dagger}$. In the case of reaction (33), ΔS° is not known experimentally [88].

4.3.6. Results of calculations

Simulations at the classical level yielded values of all ΔX° and $X^{\dagger}$ quantities (ΔG° was maintained at the experimental value as noted above). Quantal results for $G^{\dagger}$were also obtained, using path integral simulations or semiclassical results based on spectral densities from the classical simulations [14]. The calculated classical $G^{\dagger}$ and λ values were found to be in good conformity with Eq. (37), and $G_i(\eta)$ and $G_f(\eta)$ functions were close to parabolic in form (as in Fig. 2). Due to systematic deficiencies in the aqueous solvent model (a non-polarizable force field and finite coulombic cutoff ($\sim$ 10 Å)), corrections to λ were made on the basis of reference dielectric continuum models, and then $G^{\dagger}$ was corrected accordingly on the basis of Eq. (37) [14].

The calculations yielded $S^{\dagger}$ and ΔS° values of appreciable magnitude, respectively +18 eu (cal mol^{-1} K^{-1}) and +10 eu, and in contrast to the free energies, calculated S and H quantities depart substantially from the quadratic relationship given by Eq. (37). In the case of small α and also small λ_S, one expects from Eq. (37), $S^{\dagger}/\Delta S^{\circ} \sim 0.5$, whereas the calculations yielded a ratio of ~ 2 [14] (the distinction is pronounced even when taking account of the sizable estimated statistical uncertainties (± 5 eu) in the calculated entropies). For this result to be compatible with Eq. (37) would require a sizable negative value of λ_S, but in fact the simulation results indicated $\lambda_S \sim 0$. Thus, for reaction (33), as represented by the simulation and model molecular Hamiltonian [14], it was concluded that separately, the entropy and enthalpy quantities are not well accounted for by a harmonic model, whereas due to compensating effects, harmonic behavior is recovered when they are combined in the free energy quantities [14].

The final results, including the corrections noted above and the tunnelling suppression of the free energy activation barrier [14] (~ 2 kcal mol^{-1}, of which a significant fraction comes from solvent modes), are summarized in Table 10 (we note that nuclear tunnelling is expected to make only a minor (negative) contribution to $S^{\dagger}$ [92]). The tunnelling enhancement of κ_n (Γ_n, Eq. (12)) is thus roughly an order of magnitude. Estimates of nuclear tunnelling for electron exchange between TMCs are given in [12,33,34,92].

4.3.7. Comparison with experiment

With the data of Table 10 in hand, one may now make quantitative contact with experiment in terms of Eqs. (34) and (35). The experimental $S^{\dagger\prime}$ value together with the calculated $S^{\dagger}$ value and Eq. (34) yields an estimate of H_{if} (0.1–2 cm^{-1}) close to the calculated range (0.5–5 cm^{-1}). Given the estimated uncertainties, the experimental and calculated activation energies $(H^{\dagger})$are seen to be in reasonable accord as well. The primary results are summarized in Table 11.

The preceding analysis indicates the great importance of knowing $S^{\dagger}$ when it comes to unraveling the contributions to $S^{\dagger\prime}$ from an Arrhenius analysis (failure to distinguish between the $S^{\dagger\prime}$ and $S^{\dagger}$ values in Table 11 amounts to an error of a factor of ~ 20 in the H_{if} magnitude), and also offers an example in which even if

Table 10
Calculated thermodynamic quantities for the $[Ru(bpy)_2(bpy')(pro)_4(Oco(NH_3)_5)]^{3+}$ ET system [a,b,c]

$G^{\dagger}$ (kcal mol^{-1})	5.7 ± 0.1
$H^{\dagger}$ (kcal mol^{-1})	11.2 ± 1.5
$S^{\dagger}$ (eu)[d]	18.3 ± 5
ΔG° (kcal mol^{-1})	(-13.8)[e]
ΔS° (eu)[d]	10 ± 5
ΔH° (kcal mol^{-1})	-10.8 ± 1.5
λ (kcal mol^{-1})	
Total	55 ± 0.1
Solvent (λ_s)	39 ± 0.1
α[f]	-0.25

[a] Table 7 of Ref. [4], reprinted with kind permission. Copyright 2001, Wiley–VCH.
[b] The full DBA structure is displayed in Fig. 8. The ET process corresponds nominally to the reduction of Co^{3+} by an electron localized on the bpy′ ligand attached (by a carbonyl substituent) to the $(pro)_4$ bridge, leading to the low-spin (doublet) Co^{2+} final state. The $G^{\dagger}$, $H^{\dagger}$ and λ values have been corrected for systematic limitations of the solvent model (as described in detail in Ref. [14]), and $G^{\dagger}$ and $H^{\dagger}$ include contributions from quantal tunnelling.
[c] All results are taken from Ref. [14].
[d] eu $\equiv$ cal mol^{-1} K^{-1}.
[e] Constrained by a constant offset in the final state Hamiltonian (Section 4.3).
[f] $\alpha \equiv \Delta G^{\circ}/\lambda$.

ΔS° were available from experiment, it would not be a useful guide to estimating $S^{\dagger}$ (i.e. via Eq. (37)).

5. Summary and future prospects

5.1. Summary

As a result of rapidly-evolving and mutally-reinforcing advances in theoretical, experimental, and computational techniques, enormous recent progress has been achieved in quantitative, mechanistic understanding of ET processes at the molecular level. By exploiting a number of powerful quantal, semiclassical, and classical approaches (several of which are surveyed in the present chapter), it is becoming possible to give a satisfactory quantitative account of the crucial energetic and dynamic features controlling ET kinetics and to assemble them into overall ET rate constants for DBA aggregates of increasingly rich chemical complexity.

This review has focused in particular on the evaluation and analysis of the kinetic quantities primarily responsible for controlling transfer of electron between TMC, either in bimolecular processes, or in analogous intramolecular processes in which the TMCs are tethered by molecular bridging units. These quantities, including electronic coupling elements (H_{if}) and activation parameters, are formulated in a unified framework encompassing thermal and optical ET. The thermal ET treatment spans the non-adiabatic and adiabatic limits, primarily within the context of TST. The evaluation of coupling elements is based on formulations of initial (ψ_i) and final (ψ_f) states developed both for cases of resonant and non-resonant donor and acceptor sites.

Table 11
Experimental vs. calculated activation parameters[a,b]

Experiment[c]	Calculation[d]
$S^{\dagger\prime} = 5.5 \pm 0.8$ eu (cal mol^{-1} K^{-1})	$S^{\dagger} = 18.3 \pm 5$ eu
$H^{\dagger} = 9.4 \pm 0.2$ kcal mol^{-1}	$H^{\dagger} = 11.2 \pm 1.5$ kcal mol^{-1}
$\lvert H_{if}\rvert = 0.1$–$2$ cm^{-1}	$\lvert H_{if}\rvert = 0.5$–$5$ cm^{-1}

[a] Table 8 of Ref. [4], reprinted with kind permission. Copyright 2001, Wiley–VCH.
[b] See Eqs. (34) and (35).
[c] Ref. [88].
[d] Ref. [14].

Examples of computational applications of the theory are presented for several TMC-based systems, exploiting detailed electronic structure calculations (based for the most part on the all-valence-electron INDO/s method) and molecular-dynamics simulations. The TMCs sampled include cases of electronically saturated (aquo and ammine) and unsaturated (cyclopentadiene, cyclobutadiene, and 2,2′-bipyridine) ligands, and the role of metal/ligand mixing in determining overall H_{if} magnitudes is discussed in detail (including the perspective gained from superexchange theory) as well as the dependence on intersite geometry (separation distance and relative orientation). In situations where direct comparison is possible, calculated and experimental estimates of H_{if} values are in reasonable accord, and the detailed results of the calculations are shown to be of value in the analysis of the experimental data.

In selecting ψ_i and ψ_f for use within the conventional TSA, ambiguities may arise in the case of open shell TMCs, e.g. due to near-degeneracy within metal d-orbital manifolds or alternative high and low spin states, as discussed for some illustrative examples.

Detailed treatment of ET between Ru and Co coordination complexes tethered by a tetraproline spacer has led to estimates of entropy as well as enthalpy of activation, a distinction shown to be crucial when it comes to extracting the H_{if} magnitude from the Arrhenius prefactor [14].

5.2. Future prospects

The examples dealt with herein underscore the power of present-day theoretical and computational techniques applied to ET in complex molecular assemblies based on TMCs. Even more powerful and accurate treatments of ET in extended chemical systems are now beginning to appear as a result of continuous improvements in technical capabilities of electronic structure methodology [22,29–31,93,94]. While the semiempirical INDO/s

method emphasized in the present work will continue to serve as a valuable tool for evaluation of ET properties, especially for cases involving TMCs, where encouraging comparisons with ab initio results for model systems have been obtained (e.g. see Table 1), there is clearly a need for more rigorous methods for which application to complex TMC-based systems is feasible. Promising results are now available based both on ab initio wavefunction methods (Hartree–Fock (HF) [22] and correlated extensions such as symmetry-adapted-cluster configuration interaction (SAC-CI) [21]) and procedures employing density functional theory (DFT) [93,94]. Both ab initio and DFT approaches can be applied to excited state as well as ground state systems (practical realization of excited state capability for DFT is a very recent development [95,96]). Recent studies have dealt with ET involving metallo-porphyrins in photosynthetic reaction centers and a model metalloprotein system, for which H_{if} magnitudes were evaluated and analyzed [20–23]. Some of these studies included explicit treatment of excited states [20,21]. In other ab initio and DFT metalloprotein studies, alternative spin states were considered and account taken of environmental factors by use of dielectric continuum or hybrid quantum mechanical/molecular mechanics (QM/MM) techniques [93,94].

While molecular-level simulation techniques are of great value in estimating activation energetics, as illustrated in Section 4.3, the practical limitation in general to non-polarizable medium force fields introduces significant artifacts into calculated reorganization energies (an approximate correction for this defect was noted in Section 4.3). Schemes for implementing polarizable force fields have been discussed in the recent literature [97], and it is anticipated that in the near future it will be feasible to carry out fully self consistent calculations for complex ET systems, in which the mutual polarization response of the 'solute' and its environment are realistically accounted for.

Acknowledgements

This research was carried out at Brookhaven National Laboratory under contract DE-AC02-98CH10886 with the US Department of Energy and supported by its Division of Chemical Sciences, Office of Basic Energy Sciences.

References

[1] V. Balzani (Ed.), Electron Transfer in Chemistry, vols. I–V, Wiley–VCH, Weinheim, 2001.
[2] J. Jortner, M. Ratner (Eds.), Molecular Electronics, Blackwell Science, Oxford, 1997.
[3] A.P. de Silva (Ed.), Molecular-Level Electronics, vol. V, part 1, Wiley–VCH, Weinheim, 2001.
[4] M.D. Newton, in: P. Piotrowiak (Ed.), Principles and Theories, vol. I, part 1, Wiley–VCH, Weinheim, 2001, pp. 3–63.
[5] B.S. Brunschwig, C. Creutz, N. Sutin, Coord. Chem. Rev. 177 (1998) 61.
[6] R.J. Crutchley, Adv. Inorg. Chem. 41 (1994) 273.
[7] H.B. Gray, J.R. Winkler (Eds.), Biological Systems, vol. III, part 1, Wiley–VCH, Weinheim, 2001.
[8] K.D. Konstanttinos, D. Demadis, C.M. Hartshorn, T.J. Meyer, Chem. Rev. 101 (2001) 2655.
[9] (a) J.F. Endicott, Md.J. Uddin, Coord. Chem. Rev. 219 (2001) 687;
(b) J.F. Endicott, in: P. Piotrowiak (Ed.), Principles and Theories, vol. I, part 1, Wiley–VCH, Weinheim, 2001, p. 238.
[10] (a) A.A. Stuchebrukhov, R.A. Marcus, J. Phys. Chem. 99 (1995) 7581;
(b) I. Daizadeh, E.S. Medvedev, A.A. Stuchebrukhov, Proc. Natl. Acad. Sci. USA 94 (1997) 3703.
[11] M.A. Thompson, M.C. Zerner, J. Am. Chem. Soc. 113 (1991) 8210.
[12] M.D. Newton, J. Phys. Chem. 95 (1991) 30.
[13] M.D. Newton, K. Ohta, E. Zhong, J. Phys. Chem. 95 (1991) 2317.
[14] L.W. Ungar, M.D. Newton, G.A. Voth, J. Phys. Chem. B 103 (1999) 7367.
[15] J. Zeng, N.S. Hush, J.R. Reimers, J. Phys. Chem. 99 (1995) 10459.
[16] J. Zeng, N.S. Hush, J.R. Reimers, J. Am. Chem. Soc. 118 (1996) 2059.
[17] A. Broo, S. Larsson, Chem. Phys. 161 (1992) 363.
[18] I.V. Kurnikov, L.D. Zusman, M.G. Kurnikova, R.S. Farid, D.N. Beratan, J. Am. Chem. Soc. 119 (1997) 5690.
[19] C.J. Calzado, J.F. Sanz, J. Am. Chem. Soc. 120 (1998) 1051.
[20] L.Y. Zhang, R.A. Friesner, R.B. Murphy, J. Chem. Phys. 107 (1997) 450.
[21] J. Hasegawa, K. Ohkawa, H. Nakatsuji, J. Phys. Chem. B 102 (1998) 10420.
[22] Y. Ohtsuka, K. Ohkawa, H. Nakatsuji, J. Comp. Chem. 22 (2001) 521.
[23] J. Kim, A. Stuchebrukhov, J. Phys. Chem. 104 (2000) 8606.
[24] J.R. Reimers, N.S. Hush, J. Phys. Chem. 103 (1999) 3066.
[25] (a) I. Cacelli, A. Ferretti, J. Chem. Phys. 109 (1998) 8583;
(b) A. Bencini, I. Ciofini, C.A. Daul, A. Ferretti, J. Am. Chem. Soc. 121 (1999) 11418.
[26] I. Cacelli, A. Ferretti, J. Phys. Chem. 103 (1999) 4438.
[27] G.M. Pearl, M.C. Zerner, J. Am. Chem. Soc. 121 (1999) 399.
[28] M.R.A. Blomberg, P.E.M. Siegbahn, G.T. Babcock, J. Am. Chem. Soc. 120 (1998) 8812.
[29] D.T. Mainz, J.J. Klicic, R.A. Friesner, J.-M. Langlois, J.K. Perry, J. Comp. Chem. 18 (1997) 1863.
[30] R.A. Friesner, B.D. Dunietz, Acc. Chem. Res. 34 (2001) 351.
[31] I. Okazaki, F. Sato, H. Kashiwagi, J. Mol. Struct. (Theochem.) 461–462 (1999) 325.
[32] P.E.M. Siegbahn, M.R.A. Blomberg, Chem. Rev. 100 (2000) 421.
[33] N. Sutin, Prog. Inorg. Chem. 30 (1983) 441.
[34] R.A. Marcus, N. Sutin, Biochim. Biophys. Acta 811 (1985) 265.
[35] B.S. Brunschwig, N. Sutin, Coord. Chem. Rev. 187 (1999) 233.
[36] M.D. Newton, Chem. Rev. 91 (1991) 767.
[37] M.D. Newton, Adv. Chem. Phys. 106 (1999) 303 (Erratum: the factor of 1/4 in Eq. (3.27a) should be replaced by the factor 4).
[38] J. Jortner, M. Bixon, Adv. Chem. Phys. 106 (1999) 35.
[39] A.A. Stuchebrukhov, Adv. Chem. Phys. 118 (2001) 1.
[40] S.S. Skourtis, D.N. Beratan, in: P. Piotrowiak (Ed.), Principles and Theories, vol. I, part 1, Wiley–VCH, Weinheim, 2001, pp. 109–125.
[41] (a) I.R. Gould, D. Noukakis, L. Gomez-Jahn, R.H. Young, J.L. Goodman, S. Farid, Chem. Phys. 176 (1993) 439;
(b) R.A. Marcus, J. Phys. Chem. 93 (1989) 3078.

[42] J. Jortner, M. Bixon, J. Chem. Phys. 88 (1988) 167.
[43] (a) R.A. Marcus, J. Chem. Phys. 24 (1956) 966;
(b) G.K. Schenter, B.C. Garrett, D.G. Truhlar, J. Phys. Chem. B 105 (2001) 9672.
[44] P. Vath, M.B. Zimmt, D.V. Matyushov, G.A. Voth, J. Phys. Chem. B 103 (1999) 9130.
[45] C.M. Elliott, D.L. Derr, D.V. Matyushov, M.D. Newton, J. Am. Chem. Soc. 120 (1998) 11714.
[46] D.L. Derr, C.M. Elliott, J. Phys. Chem. A 103 (1999) 7888.
[47] J.N. Onuchic, D.N. Beratan, J.J. Hopfield, J. Phys. Chem. 90 (1986) 3707.
[48] M.D. Newton, N. Sutin, Ann. Rev. Phys. Chem. 35 (1984) 437.
[49] M.B. Robin, P. Day, Adv. Inorg. Chem. Radiochem. 10 (1967) 247.
[50] P.A. Cox, Chem. Phys. Lett. 69 (1980) 340.
[51] J.-J. Girerd, J. Chem. Phys. 79 (1983) 1766.
[52] B.S. Brunschwig, S. Ehrenson, N. Sutin, J. Am. Chem. Soc. 106 (1984) 6858.
[53] E.H. Yonemoto, G.B. Saupe, R.H. Schmehl, S.M. Hubig, R.L. Riley, B.L. Iverson, T.E. Mallouk, J. Am. Chem. Soc. 116 (1994) 4786.
[54] B.M. Hoffman, M.A. Ratner, J. Am. Chem. Soc. 109 (1987) 6237.
[55] B.S. Brunschwig, N. Sutin, J. Am. Chem. Soc. 111 (1989) 7454.
[56] J. Jortner, M. Bixon, T. Langenbacher, M.E. Michel-Beyerle, Proc. Natl. Acad. Sci. USA 95 (1998) 12759.
[57] S. Larsson, Theor. Chim. Acta (Berl.) 60 (1981) 111.
[58] M. Braga, A. Broo, S. Larsson, Chem. Phys. 156 (1991) 1.
[59] H.M. McConnell, J. Chem. Phys. 35 (1961) 508.
[60] S. Larsson, J. Am. Chem. Soc. 103 (1981) 4034.
[61] L.A. Curtiss, C.A. Naleway, J.R. Miller, Chem. Phys. 176 (1993) 387.
[62] (a) M.J. Shepard, M.N. Paddon-Row, K.D. Jordan, Chem. Phys. 176 (1993) 289;
(b) M.N. Paddon-Row, Acc. Chem. Res. 27 (1994) 18.
[63] M.D. Newton, R.J. Cave, in: J. Jortner, M.A. Ratner (Eds.), Molecular Electronics, Blackwell Science, Oxford, 1997, p. 73.
[64] M.D. Newton, Int. J. Quant. Chem. 77 (2000) 255.
[65] W.B. Davis, M.R. Wasielewski, M.A. Ratner, V. Mujica, A. Nitzan, J. Phys. Chem. A 101 (1997) 6158.
[66] C. Creutz, M.D. Newton, N. Sutin, J. Photochem. Photobiol. A: Chem. 82 (1994) 47.
[67] F. Salaymeh, S. Berhane, R. Yusof, R. de la Rosa, E.Y. Fung, R. Matamoros, K.W. Lau, Q. Zheng, E.M. Kober, J.C. Curtis, Inorg. Chem. 32 (1993) 3895.
[68] Y. Dong, J.T. Hupp, Inorg. Chem. 31 (1992) 3170.
[69] C.E.B. Evans, M.L. Naklicki, A.R. Rezvani, C.A. White, V.V. Kondratiev, R.J. Crutchley, J. Am. Chem. Soc. 120 (1998) 13096.
[70] S.F. Nelsen, R.F. Ismagilov, K.E. Gentile, D.R. Powell, J. Am. Chem. Soc. 121 (1999) 7108.
[71] (a) R.J. Cave, M.D. Newton, Chem. Phys. Lett. 249 (1996) 15;
(b) R.J. Cave, M.D. Newton, J. Chem. Phys. 106 (1997) 9213.
[72] N.S. Hush, Electrochim. Acta 13 (1968) 1005.
[73] H. Nakamura, D.G. Truhlar, J. Chem. Phys. 115 (2001) 10353.
[74] M. Bixon, J. Jortner, J.W. Verhoeven, J. Am. Chem. Soc. 116 (1994) 7349.
[75] N.A. Van Dantzig, D.H. Levy, C. Vigo, P. Piotrowiak, J. Chem. Phys. 103 (1995) 4894.
[76] M.C. Zerner, G.H. Loew, R.F. Kirchner, U.T. Mueller-Westerhoff, J. Am. Chem. Soc. 102 (1980) 589.
[77] M.D. Newton, in: G. Pacchioni, P.S. Bagus, F. Parmigiani (Eds.), Cluster Models for Surface and Bulk Phenomena, Plenum Press, New York, 1992, p. 551.
[78] M.D. Newton, J. Phys. Chem. 92 (1988) 3049.
[79] D.E. Richardson, H. Taube, J. Am. Chem. Soc. 105 (1983) 40.
[80] G.E. McManis, R.M. Nielson, A. Gochev, M.J. Weaver, J. Am. Chem. Soc. 111 (1989) 5533.
[81] M.D. Newton, ACS Symposium Series, in press.
[82] H. Plenio, J. Hermann, A. Sehring, Chem. Eur. J. 6 (2000) 1820.
[83] A.-C. Ribou, J.-P. Launay, M.L. Sachtleben, H. Li, C.W. Spangler, Inorg. Chem. 35 (1996) 3735.
[84] Y.-g.K. Shin, B.S. Brunschwig, C. Creutz, M.D. Newton, N. Sutin, J. Phys. Chem. 100 (1996) 1104.
[85] (a) A. Yoshimura, K. Nozaki, T. Ohno, Coord. Chem. Rev. 159 (1997) 375;
(b) X. Song, Y. Lei, S. Van Wallendal, M.W. Perkovic, D.C. Jackman, J.F. Endicott, D.P. Rillema, J. Phys. Chem. 97 (1993) 3225.
[86] R.M. Harrison, T. Brotin, B.C. Noll, J. Michl, Organometallics 16 (1997) 3401.
[87] M.E. Stoll, S.R. Lovelace, W.E. Geiger, H. Schimanke, I. Hyla-Kryspin, R. Gleiter, J. Am. Chem. Soc. 121 (1999) 9343.
[88] M.Y. Ogawa, J.F. Wishart, Z. Young, J.R. Miller, S.S. Isied, J. Phys. Chem. 97 (1993) 11456.
[89] B.R. Brooks, R.E. Bruccoleri, B.D. Olafson, D.J. States, S. Swaminathan, M. Karplus, J. Comput. Chem. 4 (1983) 187.
[90] J. Cao, G.A. Voth, J. Chem. Phys. 106 (1997) 1769.
[91] R.A. Marcus, N. Sutin, Comments Inorg. Chem. 5 (1986) 119.
[92] B.S. Brunschwig, J. Logan, M.D. Newton, N. Sutin, J. Am. Chem. Soc. 102 (1980) 5798.
[93] R.B. Murphy, D.M. Philipp, R.A. Friesner, J. Comput. Chem. 21 (2000) 1442.
[94] B.H. McMahon, B.P. Stojkovic, P.J. Hay, R.L. Martin, A.E. Garcia, J. Chem. Phys. 113 (2000) 6831.
[95] S. Hirata, T.J. Lee, M. Head-Gordon, J. Chem. Phys. 111 (1999) 8904.
[96] S.I. Gorelsky, A.B.P. Lever, J. Organometallic Chem. 635 (2001) 187.
[97] H.A. Stern, G.A. Kaminski, J.L. Banks, R. Zhou, B.J. Berne, R.A. Friesner, J. Phys. Chem. B 103 (1999) 4730.
[98] J.R. Reimers, N.S. Hush, J. Phys. Chem. 95 (1991) 9773.
[99] D.H. Oh, M. Sano, S.G. Boxer, J. Am. Chem. Soc. 113 (1991) 6880.